ELSEVIER

Thin Solid Films 366 (2000) 181–190

thin solid films

www.elsevier.com/locate/tsf

Pad porosity, compressibility and slurry delivery effects in chemical-mechanical planarization: modeling and experiments

Dipto G. Thakurta[a, b], Christopher L. Borst[a, b], Donald W. Schwendeman[c], Ronald J. Gutmann[b, d], William N. Gill[a, b,*]

[a]*Department of Chemical Engineering, Rensselaer Polytechnic Institute, Troy, NY 12180, USA*
[b]*Center for Integrated Electronics and Electronic Manufacturing, Rensselaer Polytechnic Institute, Troy, NY 12180, USA*
[c]*Department of Mathematical Sciences, Rensselaer Polytechnic Institute, Troy, NY 12180, USA*
[d]*Department of Electrical, Computer and Systems Engineering, Rensselaer Polytechnic Institute, Troy, NY 12180, USA*

Received 19 August 1999; received in revised form 18 December 1999; accepted 3 January 2000

Abstract

A chemical-mechanical planarization (CMP) model based on lubrication theory is developed which accounts for pad compressibility, pad porosity and means of slurry delivery. Slurry film thickness and velocity distributions between the pad and the wafer are predicted using the model. Two regimes of CMP operation are described: the lubrication regime (for ~40–70 μm slurry film thickness) and the contact regime (for thinner films). These regimes are identified for two different pads using experimental copper CMP data and the predictions of the model. The removal rate correlation based on lubrication and mass transport theory agrees well with our experimental data in the lubrication regime.

Keywords: Chemical mechanical planarization; Lubrication model; Polish pad properties; Wafer scale model

1. Introduction

Chemical mechanical planarization (CMP) is widely accepted for planarizing both metal and inter-level dielectric layers [1–7]. During the CMP process, a rotating wafer is pressed face down on a rotating pad while a slurry containing chemicals and abrasive particles is delivered on or up through the pad. Planarization of the wafer results from the synergistic action of the mechanical shear forces and the chemical action of the slurry [7,8]. Since the CMP process is not completely understood, physically based models are needed to provide fundamental insight into the mechanisms involved. Several CMP models have been published in the literature, with Nanz and Camilletti [9] presenting a good review of the existing models up to 1995. Some models are based on the contact mechanics of the wafer and the pad [10–16], while others are based on the slurry hydrodynamics [17–19] and lubrication theory [20,21]. A recent model developed by Tichy et al. [22] includes both lubrication hydrodynamics and contact mechanics. This paper presents a two-dimensional (2D) CMP model based on lubrication theory in which pad porosity, compressibility and slurry delivery effects are included.

Two distinct regimes of CMP operation are possible depending upon the tool, wafer, pad and slurry parameters, namely (i) the lubrication and (ii) the contact regime as depicted in Fig. 1. In the lubrication regime, which is the prime focus of the model developed in this work, a thick slurry film (~40–70 μm) separating the wafer from the pad reduces direct contact between the pad and wafer, thereby reducing scratching of the wafer surface. The fluid pressure developed in the slurry film supports the applied pressure. As the slurry film thickness increases, the fluid shear stress at the wafer surface decreases, resulting in a decreased material removal rate. Hence, a balance exists between obtaining a 'scratch-free' surface and maximizing the removal rate [21]. Low applied pressures, P_{app}, and high relative pad velocities, U, are favorable conditions for the lubrication mode of operation. The lubrication mode of operation can be used in the final 'buffing' step to give a smooth finish to the wafer surface.

In the contact regime, the wafer-pad solid-solid contact pressure supports the applied pressure. While surface scratching can occur from intimate contact between the pad and wafer, higher removal rates can be achieved. The

* Corresponding author. Tel.: + 518-276-6377; fax: + 518-276-4030.
E-mail address: gillw@rpi.edu (W.N. Gill)

0040-6090/00/$ - see front matter
PII: S0040-6090(00)00748-3

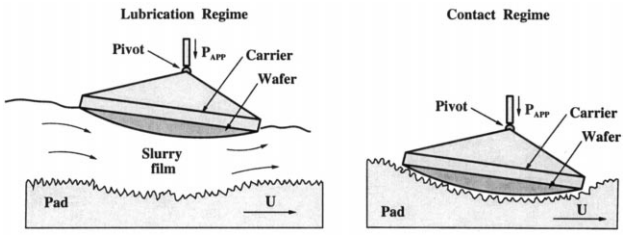

Fig. 1. Lubrication and contact regime of CMP.

contact mode of CMP is favored at high applied pressures and low relative pad velocities. Appropriate models for this regime are based on theory of contact mechanics from which the contact pressure at the wafer surface may be computed, with the contact pressure distribution related to the removal rate. Contact mechanics and stress based models also have been developed [10–16]. In this article, we identify the two regimes of CMP operation using experimental copper CMP data and model predictions.

Sundararajan et al. [21] developed a CMP lubrication model for a rigid non-porous pad. However, CMP pads, which are typically made of polyurethane, bend under the applied pressure and are also porous. Both pad bending and porosity affect the flow hydrodynamics, slurry film thickness, and angle of attack of the wafer. The shape of the wafer-pad gap changes due to pad bending. At the same time, pad porosity causes a small amount of the slurry to leak or seep into the pad underneath the wafer. In this paper, the 2D lubrication model developed by Sundararajan et al. is extended to take into account pad porosity and compressibility. For a given set of operating parameters the lubrication model predicts the slurry film thickness, the velocity distributions, and the fluid shear stress at the wafer surface. The slurry film thickness distribution is useful in determining the regime of CMP operation. If the minimum slurry film thickness is greater than the average height of pad asperities (~20–25 μm [23–25]), the operation is considered to be in the lubrication regime; if the computed film thickness is less than the height of the pad asperities, contact regime operation is more likely. Slurry velocity distributions can be used in shear stress and mass transport calculations to predict material removal rate [21] and to compute abrasive particle trajectories [26]. This paper includes computations of slurry film thickness and shear stress for hard/less-porous (for, e.g. IC 1000) and soft/more-porous (for, e.g. Suba IV) pads. (Both IC and Suba pads are manufactured by Rodel Corp., Newark, DE.)

In most CMP tool designs, the slurry is delivered on top of the pad surface. However, in tools such as the IPEC 676 [27], manufactured by IPEC-Planar, Phoenix, AZ, the slurry is introduced from the bottom of the pad. In this case, perforated pads are used to enable slurry flow up through them at a constant flow rate. Our new lubrication model also includes slurry delivery from the bottom. The average slurry film thickness and the fluid shear stress at the wafer surface is greater than when the slurry is delivered on top. Hence, a smoother surface finish is expected together with a higher removal rate.

The CMP model presented in this work is based on the theory of lubrication. Considerable simplifications in the equations governing the slurry flow may be achieved if one recognizes that the reduced Reynolds number

$$\mathrm{Re}^{*} = \frac{\rho U D}{\mu}\left(\frac{\bar{h}}{D}\right)^{2} \tag{1}$$

is small, where ρ and μ are the slurry density and viscosity, respectively, U is relative velocity between the wafer and pad, and D is the diameter of the wafer. A typical film thickness, $\bar{h}$, is of the order of micrometers which results in a value of Re^{*} in the range 10^{-2}–10^{-3}; therefore the usual assumptions in lubrication theory apply. Based on the lubrication model presented here and the mass transport model developed by Sundararajan et al. [21] the removal rate in the lubrication regime for a given pad can be correlated to $\tau_{avg}/(h_{avg}/U)^{1/3}$, where τ_{avg} is the average fluid shear stress at the wafer surface, and h_{avg} is the average slurry film thickness.

2. 2D lubrication model development

Fig. 2 illustrates the 2D lubrication model for slurry flow including the geometry of the pad and wafer. In this conventional configuration, the slurry delivery is on top of the pad. The coordinate system is fixed relative to the wafer with the origin taken to be on the undeformed pad surface directly below the center of the wafer. The wafer height is given by $y = h(x)$ measured relative to an undeformed pad and includes an angle of attack and a global curvature. A global convex curvature is often imposed by the shape of the wafer-backing film [10] and/or by applying back pressure [16] to help offset excessive material removal at the edges. The curvature is represented in terms of the protrusion at the center of the wafer, also known as the wafer dome height [17]. The wafer dome height is denoted by δ_0 and is of the order of 10 μm for an 8 inch diameter wafer. (Note that the curvature shown in Fig. 1 is exaggerated for the purpose of illustration.) The pad moves from left to right with a constant velocity U relative to the wafer and drags the slurry

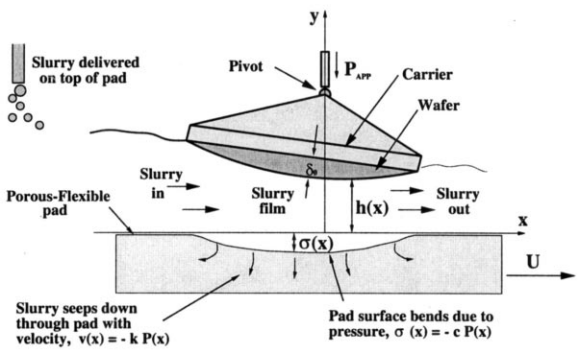

Fig. 2. Model schematic for slurry delivery on top of pad.

under the wafer. Because the gap between the pad and wafer is thin, a significant lubricating pressure $P(x)$ in the slurry film can be developed which supports a constant downward applied pressure P_{app} to the wafer and causes a deformation of the pad given by $y = \sigma(x)$. (All pressures are relative to the atmospheric pressure.) The wafer is held during CMP by a gimbaling mechanism which pivots to a stable configuration with an assumed zero moment of torque about $x = 0$ [17,21]. Finally, as the model is 2D, it does not explicitly incorporate rotation of the wafer relative to the pad and it also neglects slurry flow in the z-direction.

Models are needed to describe the deformation and porosity of the pad. It is assumed that the pad behaves, to a first approximation, as a linear spring so that the pressure $P(x)$ and pad deflection $\sigma(x)$ are related locally by Hooke's law

$$\sigma(x) = -cP(x) \tag{2}$$

where the spring constant c measures the compressibility of the pad. This model neglects bending moments in the pad which is reasonable except possibly for a small region near the edge of the pad [11]. A minus sign is included in the model so that a positive pressure results in a downward pad deflection when $c > 0$. In the gap between the pad and wafer, the x and y components of the fluid velocity are given by $u(x,y)$ and $v(x,y)$, respectively. At the wafer surface, it is assumed that fluid velocity satisfies the no-slip boundary condition and no flow penetration so that

$$u(x, h(x)) = v(x, h(x)) = 0 \tag{3}$$

At the pad, a no-slip boundary condition is assumed so that

$$u(x, \sigma(x)) = U \tag{4}$$

The y-component of the velocity at the pad is determined by the fluid pressure and the porosity of the pad k_1 and is taken to be

$$v(x, \sigma(x)) = -k_1\ P(x) \tag{5}$$

where the minus sign indicates that the seepage velocity is in the negative y-direction when $k_1 > 0$.

In certain CMP tool designs, e.g. the IPEC 676 [27], the slurry is introduced up through the pad. Fig. 3 shows the model schematic for the case when slurry is delivered from the bottom of the pad at a constant flow rate. These pads have holes (ca. 1 mm diameter) drilled through them to facilitate slurry distribution. A uniform distribution of holes provides an effective porosity of the pad k_2, which is much larger than the material porosity k_1 as given in Eq. (5). Thus, for this tool configuration, Eq. (5) is modified to

$$v(x, \sigma(x)) = k_2(P_s - P(x)) \tag{6}$$

where P_s is the pressure of the slurry delivery line. The delivery pressure must overcome the slurry fluid pressure to inject the slurry upwards into the gap. As P_{app} increases, P_s must be appropriately increased to maintain a constant slurry up-flow rate. It is noted that the IPEC 676 tool configuration with upward slurry delivery has a complex orbital

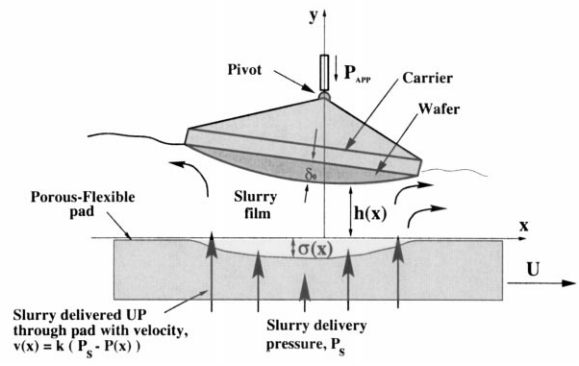

Fig. 3. Model schematic for slurry delivery up through pad.

and rotational motion of the wafer carrier. The 2D model presented here does not model these complex motions accurately but should give qualitative results for this tool. The 2D model should be regarded as a first step towards a more accurate 3D model for this tool. Such a model is under current development. An equation for the pressure $P(x)$ in the gap is given by the Reynolds equation of lubrication theory [21] which we have generalized here to include the effects of pad compressibility and porosity. The equation is

$$\frac{\mathrm{d}}{\mathrm{d}x}\left[(h-\sigma)^3\frac{\mathrm{d}P}{\mathrm{d}x}\right] = 6\mu U\frac{\mathrm{d}}{\mathrm{d}x}(h+\sigma) - 12\mu k_i(P_i - P) \tag{7}$$

where $h - \sigma = h + cP$ is the gap thickness, and where $i = 1$ with $P_1 = 0$ denotes slurry delivered on the top and $i = 2$ with $P_2 = P_s$ denotes slurry delivered up through the bottom. The equation for $P(x)$ is to be solved subject to the boundary conditions

$$P(-R_1) = P(R_1) = 0 \tag{8}$$

indicating atmospheric pressure at both the inlet and outlet, $x = -R_1$ and R_1, respectively, where R_1 is the radius of the wafer. The surface of the wafer is taken to be

$$h(x) = h_0 + S_x\left[\frac{x}{R_1}\right] + \delta_0\left[\frac{x}{R_1}\right]^2 \tag{9}$$

where h_0 is the wafer height at $x = 0$ and S_x is a 'slope' which is related to the angle of attack, $\theta = \arctan(S_x/R_1)$, of the wafer carrier. These two parameters are adjusted to balance the applied pressure and to satisfy a zero moment about $x = 0$. These two constraints are given in terms of the pressure by

$$\frac{1}{2R_1}\int_{-R_1}^{R_1} P(x)\mathrm{d}x = P_{app} \tag{10}$$

and

$$\int_{-R_1}^{R_1} P(x)x\mathrm{d}x = 0 \tag{11}$$

respectively. Eq. (7) and the boundary conditions in Eq. (8) are solved numerically using a finite difference formulation of the equations and a provisional choice for h_0 and S_x in Eq.

Table 1
Tool, wafer and slurry parameters used in base case calculations and their ranges of interest in the lubrication regime

Parameter	Range	Base case
Applied pressure, P_{app} (kPa)	7–35	20
Relative pad velocity, U (m/s)	0.5–1.0	1.0
Wafer dome height, δ_0 (μm)	5–15	10
Wafer diameter, D (in)	5–12	8
Slurry viscosity, μ (Pa s)	0.001–0.01	0.003

(9) which results in a discrete set of values for P on a grid. A method of iteration (Newton's method) is used to adjust h_0 and S_x until the integral constraints in Eqs. (10) and (11) are satisfied. The integrals are evaluated using the discrete values for P and a numerical quadrature. The solution set $\{P(x), h_0, S_x\}$ is a function of the known parameters $\{P_{app}, R_1, U, \mu, \delta_0, c, k_i, P_i\}$. Once the pressure distribution, $P(x)$, and the height parameters, h_0 and S_x, are found, the velocity distribution can be computed. Using lubrication theory, the x-component of velocity is given by

$$u(x,y) = -\frac{1}{2\mu}\frac{dP}{dx}(h-y)(y-\sigma) + U\left(\frac{h-y}{h-\sigma}\right) \qquad (12)$$

where $\sigma = -cP$. The y-component of the velocity, $v(x,y)$, follows from the equation of continuity and the boundary condition given by Eq. (5) or (6). The x-component of the velocity is used to compute the fluid-based shear stress at the wafer surface. The velocity distribution also may be used in mass-transport [21] and abrasive particle dynamics calculations.

3. Model results

In this section, results are presented for four pads with different characteristics modeled by their respective values of compressibility and porosity. For comparison purposes, one pad is chosen to be rigid and non-porous. The others model commercially available pads used in CMP tools.

Table 1 lists the range of input parameters for operation in the lubrication regime. Table 1 also gives the base parameter values used in representative calculations for the four different pads. A low applied pressure, $P_{app} = 20$ kPa, and a high relative pad velocity, $U = 1$ m/s, is chosen for the base calculations to ensure operation in the lubrication regime. Computations are made for four different types of pads, labeled 1–4 (see Table 2): pad 1 is rigid and non-porous with c and k_1 both equal to zero; pads 2 and 3 are hard and soft pads, respectively (e.g. IC 1000 and Suba IV, respectively). The hard pad is less porous than the softer pad as indicated by their values for k_1. Values for pad compressibility, c, are obtained from the literature (see, for example, Ref. [11]), but values for pad porosity, k_i, could not be found. The values for pad porosity in Table 2 are estimates which represent relatively high (pad 3) and low (pad 2) porosities. Pads 1–3 are used in tools where slurry is delivered on the top, while pad 4 is used only in tools with slurry delivery from the bottom through the pad. Drilled holes in pad 4 result in a very porous pad, with porosity k_2, which is necessary to distribute slurry properly during polishing. As described in the previous section, the slurry pressure, thickness, and velocity distributions can be computed once the Reynolds equation is solved. Figures 4 (a)–(d) show computed pad and wafer positions, slurry thickness, velocity and pressure distributions for pads 1–4, respectively, under base conditions (given in Table 1). The slurry velocity in the gap is indicated by the arrows in each plot, where the length of the arrows is normalized by U. The wafer and pad surfaces are plotted with units given on the left y-axis in micrometers. The slurry pressure, $P(x)$, in the gap is plotted as well with its units indicated on the right. The general behavior of the solution is similar for the cases in which the slurry is delivered on the top (Fig. 4 a–c). In each case, the wafer has an angle of attack, $\theta = \tan^{-1}(S_x/R_1)$, which creates a converging path for the flow from left to right through the gap. This angle increases as the pad porosity and compressibility increase. The slurry fluid pressure, $P(x)$, rises to a maximum value near the center of the wafer, with a corresponding pad deflection, $\sigma(x) = -cP(x)$, which increases for pads 2 and 3. The results for pad 4 are significantly different from the first three pads as the slurry is delivered up through the pad. The most noticeable features from Fig. 4d are: a thicker slurry film, smaller angle of attack, a flatter $P(x)$ profile, and a fanning-out slurry flow pattern. The fluid feed through the bottom for the case shown in Fig. 4d is sufficiently large to create a outflow at both the inlet and outlet which dominates the flow due to the relative velocity U. The resulting lubricating layer for this flow is nearly symmetric about $x = 0$ with an essentially zero angle of attack for the wafer.

Once the solution for a given tool configuration has been

Table 2
Pad parameters used in computations

Pad label	Type of pad	Example of pad	Slurry delivery	Compressibility, c, ($\times 10^{-10}$, m/Pa)	Porosity, k_i, ($\times 10^{-10}$, ms^{-1} Pa^{-1})
Pad 1	Rigid/non-porous	Hypothetical	Top	0	$k_1 = 0$
Pad 2	Hard/less-porous	IC 1000	Top	1.7	$k_1 = 4.0$
Pad 3	Soft/more-porous	Suba IV	Top	8.5	$k_1 = 7.0$
Pad 4	Hard/with holes	Perforated IC 1000	Bottom	1.7	$k_2 = 4000$

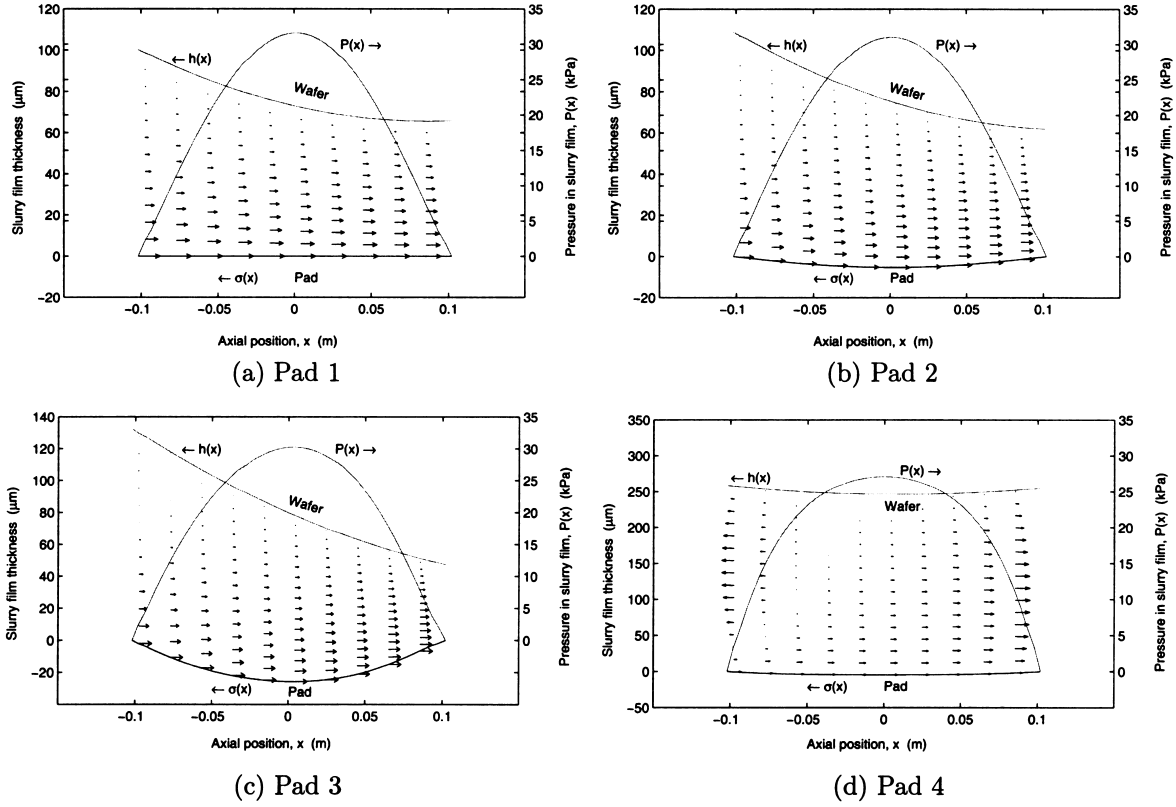

Fig. 4. Slurry velocity and pressure distributions, pad and wafer positions for pads 1–4 at base case parameter values given in Table 1 are used. $P_s = 30$ kPa for pad 4.

determined, certain CMP performance parameters can be computed. From the slurry thickness distribution, the minimum slurry film thickness, $h_{min} = \min[h - \sigma]$ can be found. This minimum usually occurs at the outlet edge due to the angle of attack of the wafer. The minimum slurry film thickness can be used to estimate the regime for CMP operation. If h_{min} is greater than the average roughness of the pad surface (~20–25 μm), then CMP operation is taken to be in the lubrication regime. Conversely, if the computed h_{min} is less than the average roughness of the pad, then the CMP operation is in the contact regime.

We can also compute an average slurry film thickness, h_{avg}, which is defined as follows

$$h_{avg} = \frac{1}{2R_1}\int_{-R_1}^{R_1}[h - \sigma]\mathrm{d}x \tag{13}$$

Using Eqs. (2), (9), and (10), Eq. (13) may further be simplified to

$$h_{avg} = h_0 + \frac{\delta_0}{3} + cP_{app} \tag{14}$$

The average slurry film thickness together with the velocity distributions can be used in an analytical mass-transport model to compute material removal rate as demonstrated in Ref. [21]. It is noted that h_{avg} could be used instead of h_{min} to estimate the regime for CMP operation, however we prefer h_{min} as it provides a more conservative estimate for the lubrication regime. In the lubrication regime, the material removal rate is proportional to the average fluid shear stress at the wafer surface, τ_{avg}. Values of τ_{avg} reported in this work (see Table 3) are calculated using

$$\tau_{avg} = \frac{1}{2R_1}\int_{-R_1}^{R_1}\mu\left|\frac{\mathrm{d}u(x,h(x))}{\mathrm{d}y}\right|\mathrm{d}x \tag{15}$$

When slurry is delivered to the top surface (conventional CMP), h_{avg} can be used to estimate the average shear stress at the wafer surface, $\tau_{avg} \sim \mu U/h_{avg}$. As h_{avg} increases, τ_{avg} decreases thereby decreasing the material removal rate. Values for h_0, S_x, and angle of attack, θ, as well as the performance parameters h_{avg}, h_{min}, and τ_{avg} are given in Table 3 for each pad at base conditions. From these values it is noted that as the angle of attack increases from pad 1 to pad 3, there is a corresponding decrease in h_{min} from 66 to 47 μm. As the front end of the wafer nears the pad surface, a transition occurs from the lubrication to contact regime. Hence, softer and more porous pads are less favorable for operation in the lubrication regime compared to harder and less porous pads. The situation is somewhat different for pad 4, whose flow is dominated by the slurry feed through the pad. In this case, the values for compressibility and porosity have a lesser effect on the transition from lubrication to

Table 3
Results for pads 1–4 for base in which the input parameters in Table 1 are used

	Pad 1	Pad 2	Pad 3	Pad 4
h_0 (μm)	73.0	75.5	79.8	247
S_x (μm)	−17.3	−23.5	− 42.4	−1.69
θ ($\times 10^6$, radians)	−170	−231	−417	−16.7
H_{avg} (μm)	76.3	82.2	100	253
h_{min} (μm)	65.5	61.9	47.4	251
τ_{avg} (Pa)	38.2	35.2	31.3	37.5
max[$P(x)$] (kPa)	31.6	31.0	30.3	27.1
max[$\sigma(x)$] (μm)	0	5.3	26	4.6
avg[$v(x(\sigma(x))$] (mm/s)	0.0	-8×10^{-3}	-14×10^{-3}	4
Slurry seepage (%)	0	5	10	−

contact. The conditions for this pad indicate the lubrication regime.

The maximum values for the slurry fluid pressure, $P(x)$, and pad deflection, $\sigma(x)$, are given in Table 3. The maximum pressure for each pad is nearly constant due the constant applied pressure, P_{app}. The maximum pad deflection, then, is approximately proportional to the value of the compressibility, c, which increases for from pads 1 to 3, and its value for pad 4 is the same as that for pad 2. (These pad deflections were seen in Fig. 4.)

An increased pad bending leads to a greater average wafer-pad separation, h_{avg}, as is also evident from Eq. (14). The increase in h_{avg} corresponds to a decrease in the average shear stress at the wafer surface, τ_{avg}, for pads 1–3.

The shear stress for pad 4 is comparable to pad 1, in spite of a larger h_{avg}. This indicates that slurry delivery through the pad allows a larger τ_{avg} together with a high h_{avg}, leading to a desirable higher removal rate and reduced scratching in the lubrication regime. In addition, the slurry film thickness depends strongly on the slurry delivery pressure, P_s. In this case, $P_s = 30$ kPa, which gives an average slurry up-flow rate, avg[$v(x, \sigma(x))$] = 4 mm/s. Due to the porosity of the pad, a certain amount of slurry seeps underneath the pad. Table 3 gives the average leakage velocity at the pad surface, avg[$v(x,\sigma(x))$] and the percent slurry seepage, which is determined by the ratio of the volume flow rate through the pad to that at the inlet. The negative sign in the leakage velocity for pads 2 and 3 implies that the slurry is seeping in the negative y-direction. (Pad 1 is non-porous with zero leakage.) As pad porosity increases, the leakage correspondingly increases (pads 1–3).

Fig. 5 shows the effect of the applied pressure and the pad velocity on h_{avg}, h_{min}, and τ_{avg} for pads 2 and 3. There are three curves in each plot corresponding to $U = 0.5$, 1.0, and 1.5 m/s. The curves are in agreement with earlier observations. For example, pad 3 bends more than pad 2, thus increasing the average pad-wafer separation, h_{avg}. Also, pad 3 has a larger angle of attack, which implies that the front edge of the wafer dips closer to the pad leading to a smaller h_{min}. When h_{min} becomes less than the height of the pad asperities, CMP operation is in the contact regime as indicated in Fig. 5c,d by the 25 μm high shaded region. For example, for $P_{app} \gtrsim 20$ kPa and $U = 0.5$ m/s, CMP with pad 3 is in the contact regime. For comparison, pad 2, which is a harder pad, does not reach the contact regime until ~30 kPa (for $U = 0.5$ m/s). The average fluid shear stress on the wafer surface is lower for pad 3 due to the a larger h_{avg}.

The behavior of the CMP performance parameters for pads 2 and 3 are compared to those for the rigid/nonporous pad 1 in Fig. 6. In this figure we note similar trends in the behavior as observed before, namely, the average film thickness is larger for more compressible pads, the minimum film thickness falls below the average pad asperity heights for the softer and more porous pads at a lower P_{app}, and the average shear stress increases with increasing P_{app}.

Fig. 7 compares the two different slurry delivery methods using pads 2 and 4 which have equal values of pad compressibility. Slurry is delivered on the top for pad 2, whereas the slurry is pumped up through the bottom of pad 4. A larger film thickness is observed for pad 4, especially at lower values of P_{app}. The curves of h_{avg} and h_{min} for pad 4 are nearly the same as the wafer has a very small angle of attack for bottom delivery. The curve for the average shear stress flattens out for pad 2, while the curve for pad 4 increases almost linearly. As noted earlier, slurry delivery from the bottom appears to be advantageous for CMP operation in the lubrication regime while maintaining a higher shear stress. A thicker film reduces the chances of scratching, while a higher shear stress leads to higher removal rates. It is important to add that all solutions for pad 4 shown in Fig. 7 have a slurry delivery rate of avg[$v(x, \sigma(x))$] = 1 mm/s. A constant delivery rate is usually maintained by a constant volume displacement pump. Thus, a higher slurry delivery pressure is required at a higher P_{app} to maintain the same slurry rate. For example, a P_s of 12.3 and 31.9 kPa at P_{app} of 10 and 30 kPa, respectively, are needed to maintain the same delivery rate of 1 mm/s.

4. Experimental results

Polishing experiments were performed over a wide range of P_{app} and U to identify the two regimes of CMP operation. Five-inch wafers with blanket copper films were polished using a IPEC 372M CMP tool. The diameter of the polishing table is approximately 57 cm and the eccentric distance between the polishing head and the center of the polishing table is 17.2 cm. The polishing table and the wafer were rotated in the same direction at equal speed for all the experiments. The applied pressure was varied between 1–6 psi, while the table/carrier speed ranged from 20 to 60 rev./min. These values correspond to $P_{app} \simeq 7$–42 kPa and $U \simeq 0.36$–1.08 m/s, respectively. The slurry used has three components: (a) an oxidizing agent, potassium ferricyanide-4 wt.%, (b) a complexing agent, ammonium hydroxide-3 vol.%, and (c) abrasive, alumina particles-2.5 wt.% (0.05

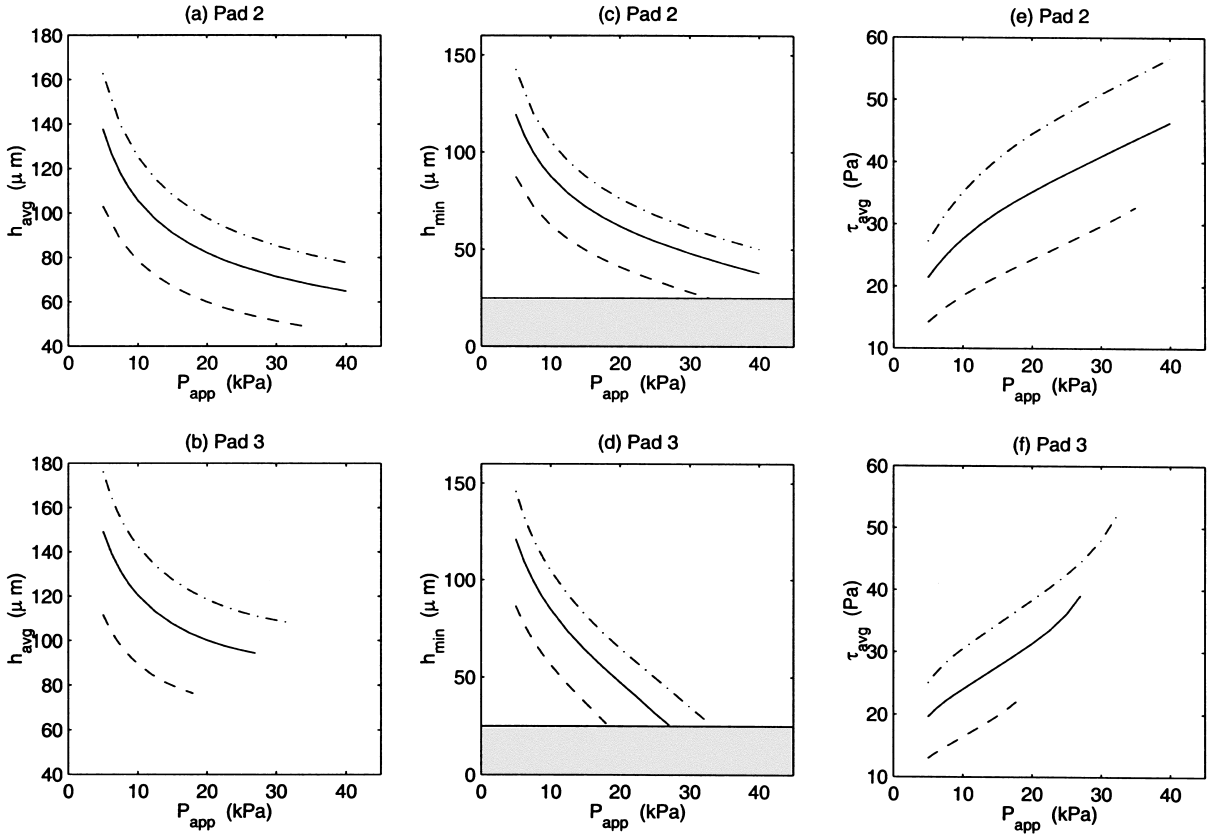

Fig. 5. Effect of P_{app} and U ($U = 0.5$ m/s, (- - -); $U = 1.0$ m/s, (—); $U = 1.5$ m/s, (-·-·-) on h_{avg}, h_{min}, and τ_{avg} for pad 2 and pad 3 (slurry delivered on top of pad). Other parameters used for the above computations are: $D = 8$ in, $\delta_0 = 10$ μm, $\mu = 0.003$ Pa s. Slurry delivery is on the top of pad in all cases shown.

μm nominal diameter). De-ionized water is added to the above to make up the slurry. The effects of the individual components of the slurry are discussed elsewhere [21]. The slurry is delivered at 200 ml/min on top of the pad. Polishing experiments were performed using two different pads, a IC 1000 without any perforations or grooves and a Suba 500. The copper removal rate, *RR*, is calculated from pre- and post-polish sheet resistance measurements using a four-point probe.

A dimensional analysis of the Reynolds equation indicates that for a given pad the slurry film thickness, $\bar{h}$, approximately scales as

$$\bar{h} \propto \sqrt{\frac{\mu U D}{P_{app}}} \tag{16}$$

The above equation is an approximation because $\bar{h}$ also depends on values of c and k_1 of the pad. Also, Eq. (16)

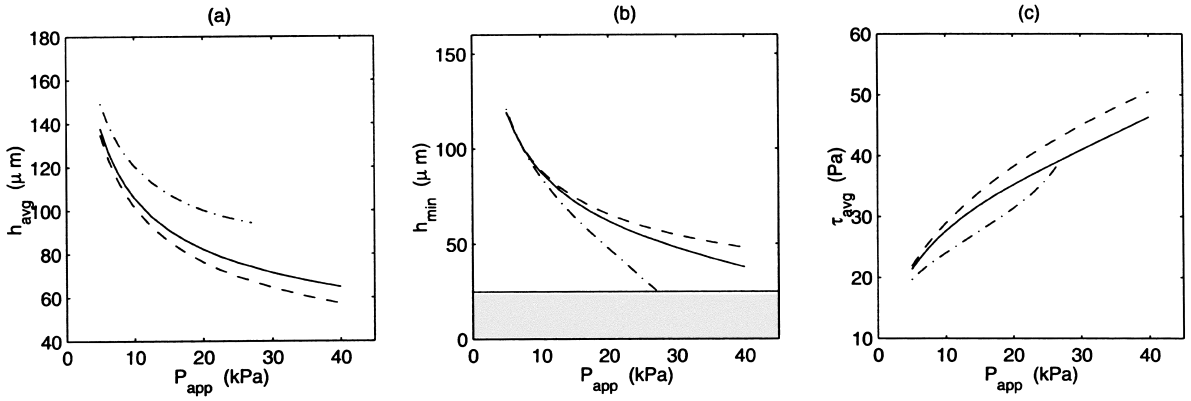

Fig. 6. Comparison of h_{avg}, h_{min}, and τ_{avg} (a–c) for pad 1 (- - -), pad 2 (—), and pad 3 (-·-·-) for different values of P_{app}. Other parameters used for the above computations are: $U = 1$ m/s, $D = 8$ in, $\delta_0 = 10$ μm, $\mu = 0.003$ Pa s. Slurry delivery is on the top of pad in all cases shown.

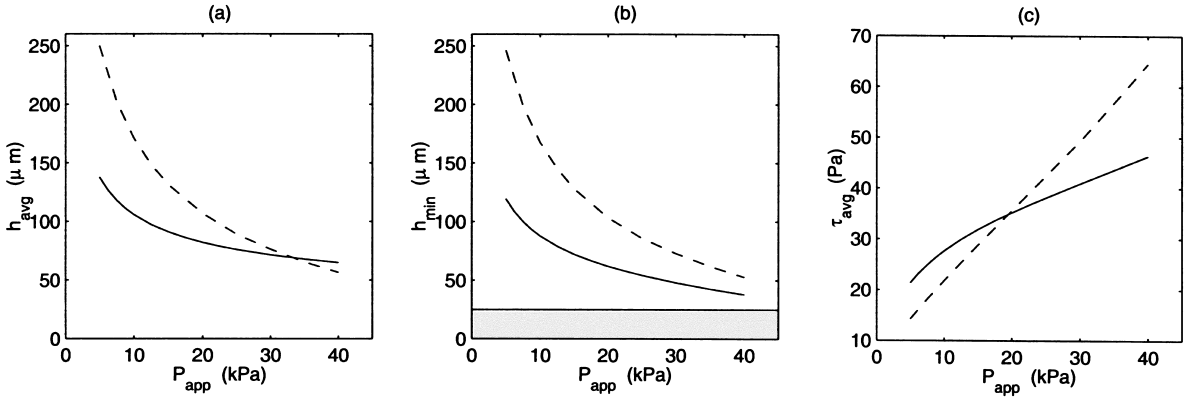

Fig. 7. Comparison of h_{avg}, h_{min}, and τ_{avg} (a–c) for slurry delivery from top (—) and bottom (- - -) using pads 2 and 4, respectively. Other parameters used for the above computations are: $U = 1$ m/s, $D = 8$ in, $\delta_0 = 10$ μm, $\mu = 0.003$ Pa s. Note: A pad with holes is used when the slurry is delivered from the bottom. Slurry is delivered at a constant rate of 1 mm/s at all P_{app} for pad 4.

holds only for slurry delivery on top of pad. As the wafer diameter, D, and the slurry viscosity, μ, are fixed in the experiments, the slurry film thickness is approximately proportional to $(U/P_{app})^{-1/2}$ (see Eq. (16)).

Fig. 8 shows a plot of normalized copper removal rate, RR/U against $(U^*/P_{app}^*)^{1/2}$. The normalized removal rate, obtained by dividing the removal rate by the relative pad velocity, represents the amount of material removed (in nm) per meter of the pad passing underneath the wafer. The other symbols, U^* and P_{app}^* are dimensionless relative pad velocity and applied pressure, respectively and are given by $U^* = U/U_{ref}$ and $P_{app}^* = P_{app}/P_{ref}$, where $U_{ref} = 1$ m/s, and $P_{ref} = 20$ kPa. The x-axis of Fig. 8 is proportional to the thickness of the slurry film, $\bar{h}$, for a given pad. The data in the contact regime are marked using triangles, whereas circles show the data in the lubrication regime. For both pads, the lubrication regime is characterized by the flatter tail of the data, where the slurry film thickness is larger. The contact regime has a steeper slope, which indicates a stronger dependence of RR/U on $(U^*/P_{app}^*)^{1/2}$. Also in the contact regime, the slope for the harder pad (IC 1000) is more steep than that for the softer pad (Suba 500). Arrows 1 and 2 mark the transition between the two regimes for the IC 1000 and Suba 500 pad, respectively.

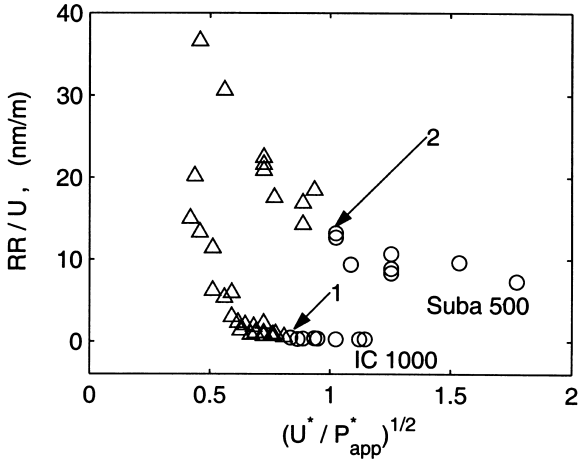

Fig. 8. Plot of normalized removal rate, RR/U, against $(U^*/P_{app}^*)^{1/2}$ for IC 1000 and Suba 500 pads, where $U^* = U/U_{ref}$ and $P_{app}^* = P_{app}/P_{ref}$, with $U_{ref} = 1$ m/s, and $P_{ref} = 20$ kPa. The triangle and circle symbols show the contact and lubrication regimes, respectively. The arrows mark the transition into the lubrication regime.

Computed h_{min} and h_{avg} for the IC 1000 pad (point 1) are 19 and 37 μm, respectively, and that for Suba 500 (point 2) are 21 and 47 μm, respectively. The input parameters for these computations are: $D = 5$ inch, $\delta_0 = 5$ μm, and $\mu = 0.001$ Pa s. The values of c and k_1 for IC 1000 and Suba 500 used are tabulated in Table 4. The computed values of h_{min} are in the order of the average pad roughness at the transition of the regimes. Toward the right of the arrows, $\bar{h}$ increases and one goes into the lubrication regime. The Suba 500 curve is shifted towards the right because a higher U and/or lower P_{app} is needed with a softer pad for operation in the lubrication regime. These results are in agreement with our model.

In the lubrication regime, the removal rate can be predicted using the fluid dynamic model presented here together with the mass transport model developed by Sundararajan et al. [21]. The present model gives the velocity components in the slurry, which in turn gives the shear stress at the wafer surface, τ_{avg}, and the average mass transport boundary layer thickness, Δ_{avg}, from the model in [21]. According to the mass transport model, the removal rate is proportional to τ_{avg} and is inversely proportional to Δ_{avg}, and

Table 4
IC 1000 and Suba 500 pad parameters used in computations

Pad	Compressibility, c ($\times 10^{-10}$, m/Pa)	Porosity, k_1 ($\times 10^{-10}$, ms^{-1} Pa^{-1})
IC 1000	1.7	4.0
Suba 500	4.0	7.0

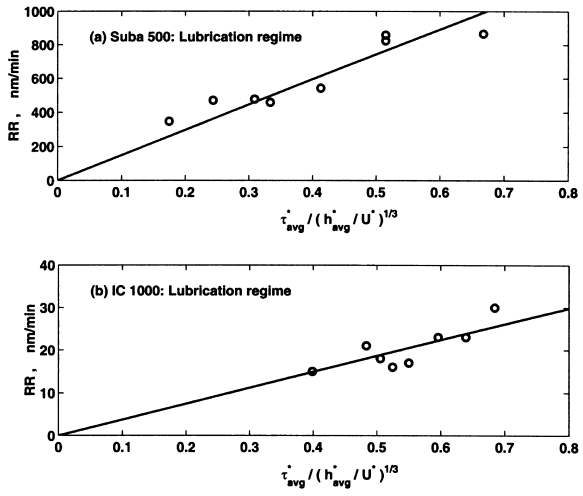

Fig. 9. The removal rate, *RR*, is proportional to $\tau_{avg}^*/(h_{avg}^*/U^*)^{1/3}$ for both (a) Suba 500, and (b) IC 1000 pads in the lubrication regime. The (*) represents dimensionless quantities: $\tau_{avg}^* = \tau_{avg}/\tau_{ref}$, $h_{avg}^* = h_{avg}/h_{ref}$ and $U^* = U/U_{ref}$, with $\tau_{ref} = 40$ Pa, $h_{ref} = 25$ μm, and $U_{ref} = 1$ m/s.

Δ_{avg} is proportional to $U^{1/3}$ and inversely proportional to $h_{avg}^{1/3}$. The removal rate decreases as Δ_{avg} increases because a larger Δ_{avg} offers more resistance to mass transfer of the dissolved copper species away from the wafer surface. Hence

$$RR \propto \frac{\tau_{avg}}{\Delta_{avg}} \propto \frac{\tau_{avg}}{(h_{avg}/U)^{1/3}} \quad (17)$$

The constants of proportionality in Eq. (4) depend on the input parameters, including c and k_1. There is also an adjustable parameter in the mass transfer model that accounts for the effects of the abrasive particles and the characteristics of the pad on the removal rate. The model does not predict this parameter but it can be determined experimentally. For the purposes of this paper, we show a correlation between the removal rate and $\tau_{avg}/(h_{avg}/U)^{1/3}$. The data points in Fig. 9a,b show the removal rate for the Suba 500 and IC 1000 pads, respectively, for various values of $\tau_{avg}^*/(h_{avg}^*/U^*)^{1/3}$, where the star superscript represents dimensionless quantities (see the figure caption). These data points correspond to the points in Fig. 1 considered to be in the lubrication regime (data points marked by circles in the plot) and thus are expected to behave as predicted by the lubrication model. The line in each figure is a least-squared fit for each data set and indicates a good correlation.

We note that the Suba 500 pad has a significantly higher removal rate as compared to the IC 1000 pad, and that this difference can not be predicted by the effects of compressibility and porosity alone using the available models. There are additional abrasive effects that have not been modeled including pad roughness, partial contact, and particle mechanics, and these effects are believed to be important especially for CMP operation near the border between the lubrication and contact regimes.

5. Summary and conclusions

A 2D wafer-scale CMP model based on lubrication theory was developed which includes pad compressibility, pad porosity and means of slurry delivery. The model can predict the slurry film thickness for given operating parameters. The slurry film thickness was used to determine the regime of CMP operation. Low P_{app}, high U, low pad compressibility and porosity, and slurry delivery from bottom favors operation in the lubrication regime, where a thicker film of slurry separates the wafer and the pad. This thick film reduces wafer scratching but also reduces the removal rate. On the other hand, there is more contact between the wafer and pad in the contact regime and high polish rates are obtained. The contact regime is favored at high P_{app}, low U, high pad compressibility and porosity.

Copper CMP experiments clearly identified the regimes for two commercial pads. The model prediction that a higher U and/or a lower P_{app} is necessary to go into the lubrication regime with a softer pad is validated by the experiments. In the lubrication regime, the removal rate was correlated to $\tau_{avg}/(h_{avg}/U)^{1/3}$, which was verified experimentally. The unexpected higher removal rate with the more compressible pad is not currently well understood.

Acknowledgements

This work was supported by the Center of Interconnect Science and Technology (CAIST), Semiconductor Research Corporation (SRC) contract number 97-IC-448. The authors would also like to thank T. Bibby (IPEC-Planar) for helpful discussions and CMP tool information.

References

[1] W.J. Patrick, W.L. Guthrie, C.L. Standley, P.M. Schiable, J. Electrochem. Soc. 138 (1991) 1778.
[2] F.B. Kaufman, D.B. Thompson, R.E. Broadie, et al., J. Electrochem. Soc. 138 (1991) 3460.
[3] S. Sivaram, H. Bath, R. Leggett, A. Maury, K. Monnig, R. Tolles, Solid State Technol. 35 (1992) 87.
[4] H. Landis, P. Burke, W. Cote, et al., Thin Solid Films 220 (1992) 1.
[5] I. Ali, S.R. Roy, G. Shinn, Solid State Technol. 37 (1994) 63.
[6] J.M. Steigerwald, R. Zirpoli, S.P. Murarka, D. Price, R.J. Gutmann, J. Electrochem. Soc. 141 (1994) 2842.
[7] J.M. Steigerwald, S.P. Murarka, R.J. Gutmann, Chemical Mechanical Planarization of Microelectronic Materials, Wiley–Interscience, New York, 1997.
[8] J.M. Steigerwald, Ph.D. Thesis, Rensselaer Polytechnic Institute, USA, 1995.
[9] G. Nanz, L.E. Camilletti, IEEE Trans, Semiconductor Manufacturing 8 (1995) 382.
[10] S.R. Runnels, P. Renteln, Dielectric Sci, Technol. (1993) 110.
[11] R. Baker, in: Electrochem. Soc. (ECS), *1996 Fall Meeting extended abstracts (EA 96-2).* 7 Oct., 1996.
[12] D. Wang, J. Lee, K. Holland, T. Bibby, T. Cale, J. Electrochem. Soc. 141 (1997) 2843.

[9] G. Nanz, L.E. Camilletti, IEEE Trans, Semiconductor Manufacturing 8 (1995) 382.
[10] S.R. Runnels, P. Renteln, Dielectric Sci, Technol. (1993) 110.
[11] R. Baker, in: Electrochem. Soc. (ECS), *1996 Fall Meeting extended abstracts (EA 96-2) 7 Oct* 1996.
[12] D. Wang, J. Lee, K. Holland, T. Bibby, T. Cale, J. Electrochem. Soc. 141 (1997) 2843.
[13] D. Wang, J. Lee, K. Holland, T. Bibby, S. Beaudoin, T. Cale, J. Electrochem. Soc. 144 (1997) 1121.
[14] C. Srinivasa-Murthy, D. Wang, S.P. Beaudoin, T. Bibby, K. Holland, T. Cale, Thin Solid Films, 308– 309 (1997) 533.
[15] O.G. Chekina, L.M. Keer, H. Liang, J. Electrochem. Soc. 145 (1998) 2100.
[16] D.G. Thakurta, S.P. Murarka, W.N. Gill, unpublished.
[17] S.R. Runnels, L.M. Eyman, J. Electrochem. Soc. 141 (1994) 1698.
[18] S.R. Runnels, J. Electrochem. Soc. 141 (1994) 1900.
[19] P.Y. Bramono, L.M. Racz, in: Proc 3rd Int. CMP for ULSI Multilevel Interconnection Conf. (CMP-MIC), Feb. 19–20, 1998, p. 185.
[20] T. Nakamura, K. Akamatsu, N. Arakawa, Bull. Japan Soc. Prec. Eng. 19 (1985) 120.
[21] S. Sundararajan, D.G. Thakurta, D.W. Schwendeman, S.P. Murarka, W.N. Gill, J. Electrochem. Soc. 146 (1999) 761.
[22] J. Tichy, J.A. Levert, L. Shan, S. Danyluk, J. Electrochem. Soc. 146 (1999) 1523.
[23] M. Bhushan, R. Rouse, J.E. Lukens, J. Electrochem. Soc. 142 (1995) 3845.
[24] D. Stein, D. Hetherington, M. Dugger, T. Stout, J. Electron. Mater. 25 (1996) 1623.
[25] K. Nakamura, S. Kishii, Y. Arimoto, Jpn. J. Appl. Phys. 36(1 (3B)) (1997) 1525.
[26] D. Bramono, J. Coppeta, L. Racz, C. Rogers, Proc 4th Int. CMP for ULSI Multilevel Interconnection Conf. (CMP-MIC), Feb. 11–12, 1999, p. 159.
[27] P. Parikh, J. Lee, D. Kreager, H. Nguyen, J. Yang, K. Holland, in: Proc. 2nd Int. CMP for ULSI Multilevel Interconnection Conf. (CMP-MIC), Feb. 13–14, 1997, p. 69.